Preprint PFC/JA-81-13

CYCLOTRON EMISSION FROM INTENSE RELATIVISTIC ELECTRON BEAMS IN UNIFORM AND RIPPLED MAGNETIC FIELDS

R. E. Shefer and G. Bekefi

June 1981

CYCLOTRON EMISSION FROM INTENSE RELATIVISTIC ELECTRON BEAMS IN UNIFORM AND RIPPLED MAGNETIC FIELDS*

R. E. Shefer and G. Bekefi

Department of Physics and Research Laboratory of Electronics

Massachusetts Institute of Technology

Cambridge, Massachusetts 02139

ABSTRACT

Millimeter wave emission from intense, relativistic electron beams ($V \simeq 1MV$, $I \simeq 5kA$) propagating in uniform and rippled magnetic fields has been studied experimentally at frequencies ranging from 8 to 140GHz. For beams propagating in a uniform guiding magnetic field, the measured spectra correspond to those predicted theoretically for the unstable cyclotron maser (gyrotron) modes. Superimposing a periodic transverse magnetic field (a wiggler), the power in these modes is enhanced by one to two orders in magnitudes, due to the additional transverse electron velocity acquired by the electrons. In our system the wiggler-enhanced cyclotron maser instability dominates over other radiation mechanisms, such as the collective (Raman) free electron laser instability, which has not been detected.

---

*This work was supported in part by the U.S. Air Force Office of Scientific Research under Grant AFOSR-77-3143 and in part by the National Science Foundation under Grant ENG79-07047

I. INTRODUCTION

During the past ten years, many experiments[1] have been carried out concerning the emission of centimeter, millimeter and submillimeter wavelength radiation from intense (I≈1-25kA), relativistic (V≈0.2-3MV) electron beams propagating in uniform and rippled magnetic fields. To achieve stimulated emission, two classes of electron beam instabilities have been exploited. These are the slow and fast cyclotron[2] instabilities on the one hand, in which the radiation is characteristic of the electron gyrofrequency and its harmonics; and the free electron laser instabilities[3] on the other hand, whose emission frequency is governed by the period of the rippled magnetic field. In both mechanisms the free energy for the instability is supplied by the transverse component of momentum of the beam electrons, which they acquire at the gun or by traversing the wiggler (or by a combination of the two). It is noteworthy that in the parameter regime of intense pulsed electron beams, the growth rates of the two classes of instabilities are of the same order of magnitude. Thus, in a system in which the electron beam is subjected simultaneously to a uniform longitudinal magnetic guide field and a wiggler field, the cyclotron and free electron laser instabilities may well be present at the same time. Therefore, detailed spectral studies with and without the wiggler field are necessary to unequivocally differentiate between the two emission mechanisms.

In this paper we describe spectral studies at frequencies ranging from 8 to 140GHz of the intense radiation emanating from pulsed relativistic electron beams carrying currents of 1 to 10kA at voltages of 0.6 to 1.3MV. The experimental parameters are summarized in Table 1. For beams propagating in uniform longitudinal

fields of 6 to 12kG, the observed discrete spectra agree well with the theoretically predicted cyclotron maser modes under conditions of maximum growth rate. Superposition of wiggler fields having 4 or 6cm periodicities and amplitudes ranging from zero to ~1kG leads to an intensity enhancement of the cyclotron maser modes by as much as a factor of 50. This is ascribed to the additional transverse velocity acquired by the electrons in traversing the periodically varying field. Radiation due to the free electron laser mechanism has not been identified in our system.

II EXPERIMENTAL ARRANGEMENT

The experimental arrangement is illustrated in Fig. 1a. A Physics International Pulserad 110A electron accelerator delivers a voltage pulse V of up to 1.5MV with a maximum current I of 35kA, and with a pulse width of 30ns. The accelerator energizes a foilless,[4] field emission diode comprised of a graphite cathode and a single accelerating anode. The cylindrical cathode together with the concentric stainless-steel anode cylinder are drawn to scale in Fig. 1b for two slightly different gun arrangements used in our experiments. Both diodes generate a hollow, annular electron beam, the conically shaped cathode giving a somewhat thicker beam. The use of witness plates and limiting apertures of various radii placed in front of the guns allow us to determine the beam profiles. From these, and the measured beam current and beam voltage we infer the electron density N, and thus the electron plasma frequency $\omega_p=[Ne^2/m_0\varepsilon_0\gamma]^{1/2}$, where m_0 is the electron rest mass and $\gamma=1 + eV/m_0c^2$.

The beam emitted from the electron gun propagates down an evacuated stainless-steel drift tube of 2cm inner diameter and 70cm

long. Both the gun and the drift tube are immersed in a uniform, axial guiding field of a 100cm long solenoid which provides a variable magnetic field of up to 21kG. The solenoid is energized by a 3.75μF, 4kV capacitor bank having a rise time of ~16ms. This means that during the short time of 30ns the relativistic beam is on, the magnetic field is essentially constant. After passage through the solenoid, the beam is allowed to expand in the fringing magnetic field and is collected on the beam dump, where the current is measured with a low-inductance current viewing probe.

The drift tube acts as a cylindrical waveguide for the emitted radiation which is guided out of the system by means of a conical horn 7.5cm in diameter and 21cm long. The quartz lens (focal length=21cm) at the end of the horn collimates the radiation and also provides the vacuum seal.

In a series of experiments (see Table 1) a coaxial stainless-steel center conductor with an outer radius of 0.397cm was placed in the drift tube in order to transform the cylindrical waveguide into a coaxial transmission line and thus change the electromagnetic mode structure. It was held in position at the diode end by three thin molybdenum legs (which grounded the conductor), and by thin ceramic legs at the beam dump end of the drift tube (which permitted free passage of any electromagnatic radiation). To insure a smooth transition, the center conductor was gently tapered at the diode end.

The centimeter and millimeter wave emission was studied in three frequency ranges 8-12GHz (X-band), 26-40GHz (Ka-band) and 75-140GHz (R and N bands), using a variety of diagnostics. The total power in a given frequency band was obtained[5] by placing a standard gain receiving horn of known gain G_r at a distance R

from the conical transmitting horn of gain G_t. Using the radar formula,

$$P_e = (16\pi^2 R^2/\lambda^2 G_e G_r)\ P_r(\theta_0,\phi_0) \tag{1}$$

we obtain the emitted power P_e from the measured, received power, $P_r(\theta_0,\phi_0)$. The unknown gain G_t is derived by an angular scan of the emitted power and use of the formula

$$G_t = 4\pi P_r(\theta_0,\phi_0)\left\{\int_0^{\pi} P_r(\theta,\phi)\sin\theta\, d\theta\, d\phi\right\}^{-1} \tag{2}$$

The spectral content of the emitted radiation was explored in the following ways. In the X and Ka band frequency ranges we used waveguide dispersive lines[5] and measured the time t required by an electromagnetic pulse of frequency ω to traverse a length L of waveguide. Knowledge of the cutoff frequency ω_c of the TE_{01} mode of the dispersive line, and use of the formula

$$\omega = \omega_c[1 - (L/ct)^2]^{-1/2} \tag{3}$$

yields the desired value of the frequency ω. The dispersion of the system $|d\omega/dt|$ and its resolution $|d\omega/dt|\Delta t$ (where Δt is the radiation pulse width) can be computed from Eq. (3). In the X-band range of frequencies the resolution is found to be approximately ±0.5GHz and in the Ka-band regime, approximately ±1.5GHz.

In the 75-140GHz range of frequencies the spectra were studies by means of a grating spectrometer.[6] The aluminum grating has a grating spacing of 0.28cm, a blaze angle of 33° and a theoretical resolving power of 54. The measured values of resolving power range between 40 and 70 depending on the frequency. The spectrometer insertion loss is 15dB/GHz and is almost independent of frequency in the measured range of 75GHz-110GHz.

Commercial microwave diode detectors set in broadband coaxial or waveguide mounts were used in all three frequency ranges and are listed in Table 1. Special care was taken in their absolute power calibration. In each frequency band, the crystal sensitivity (mV per mW) was determined at a large number of discrete frequencies using variable frequency sources and absolutely calibrated bolometers. Moreover, since the sensitivity depends on the input power level (because of the different nonlinear regimes in which crystals tend to operate) the calibrations were made at several discrete input powers. During operation, the crystal detectors were housed either in an electrically shielded room which also contained the fast storage oscilloscopes (Tektronix 7633) on which all signals were displayed; or they were carefully shielded by enclosing them in separate Faraday cages. The microwave power emitted by the relativistic electron beam is typically in the range of 10^3-10^6W, whereas the crystal detector operates in the range of tens of milliwatts. Thus, the emitted power level must be brought down to acceptable levels using precision calibrated attenuators. Figure 2 shows a typical shot which exhibits the beam voltage, beam current and the emitted microwave power. The microwave signal has a FWHM of approximately 15ns and is somewhat narrower than the 30ns voltage pulse.

One may well inquire about the beam profile after passage through the solenoid and after the wave emission process has terminated. Witness plates show that the beam is a well-defined annulus and shows no signs of instability. This is equally true when the beam is allowed to traverse the 70cm long periodic wiggler field described in section IV. In this respect our studies differ from those reported by other researchers[7] who observed serious beam deterioration after its passage through a 2m long wiggler

field.

III. SPECTRAL STUDIES IN A UNIFORM, AXIAL MAGNETIC FIELD

The observed microwave emission originates from the uniform magnetic-field region of the drifting electron beam. This has been verified in the following way. A movable wire mesh transparent to the electron beams but highly reflective to the radiations was placed in the drift tube. When the mesh is situated near the electron gun it has virtually no effect on the intensity of the emitted radiation. However, when it is moved to the far end of the drift tube, near the beam dump, the microwave signal is strongly attenuated, indicating that neither the electron gun nor the beam dump are regions of microwave emission.

The radiation intensity is a sensitive function of the axial, guiding magnetic field B_z. This is illustrated in Fig. 3 which represents a plot of the total power emitted in 75-140GHz band as a function of B_z. The emission is seen to be sharply peaked at a value of 9.4kG. Similar results are obtained for the other frequency regimes, but the peaking in power occurs at different values of magnetic field. Line 6 of Table 1 lists these critical magnetic fields under the different experimental conditions, and line 9 gives the corresponding levels of emitted power.

We now examine the emission spectra with B_z set at the critical values discussed in the foregoing paragraph. Figure 4 shows the spectral characteristics in the X and Ka-band frequency ranges as measured by means of dispersive lines. We note that in each band there is a single strong resonance which we shall interpret momentarily as a cyclotron maser mode (the much weaker, secondary spikes have not been analyzed by us). The relative line-width

$\Delta\omega/\omega$ of the resonances is approximately 0.1. The results presented in Fig. 4 refer to the systems 2 and 3 of Table 1. Similar observations were made for the waveguide systems 1 and 4 but the resonances now occurred at different frequencies. Figure 5 represents the spectral characteristics in the 75-140GHz regime as measured with the grating spectrometer. Three features can be identified in this spectrum occurring at 75, 93, and 113GHz.

We shall show that the above spectral observations made at the critical magnetic fields corresponding to peak power output are consistent with the cyclotron maser mechanism, occurring at its maximum growth rate. We have not addressed the problem of emission at values other than at these critical magnetic fields.

Efficient cyclotron maser interaction occurs when the phase velocity $\omega/k_{\parallel}$ of the Doppler shifted cyclotron frequency, or one of its harmonics,

$$\omega = s\Omega_0/\gamma + k_{\parallel}c\beta_{\parallel} \qquad (s=1,2,3\ldots) \qquad (4)$$

equals the phase velocity of an electromagnetic waveguide mode

$$k_{\parallel}^2c^2 = \omega^2 - \omega_c^2. \qquad (5)$$

Here ω and $k_{\parallel}$ are the wave frequency and axial wave number, respectively; $\Omega_0 = eB_z/m_0$ is the nonrelativistic cyclotron frequency, s is the harmonic number, $\gamma=(1-\beta_{\parallel}^2-\beta_{\perp}^2)^{-1/2}$ is the beam energy, $\beta=v/c$ and ω_c is the cutoff frequency of a mode of the cylindrical waveguide, or the coaxial transmission line, as the case may be (see Table 1). We note that the annular electron beam "loads" the waveguide (or transmission line) causing an upshift of the cutoff frequency compared to its value ω_{c0} when empty. We calculate the corrected cutoff frequency from the equation

$$\omega_c = \left[\omega_{c0}^2 + \omega_{pe}^2\right]^{1/2} \tag{6}$$

where ω_{pe} is an "effective" plasma frequency, and is defined as follows:

$$\omega_{pe}^2 = \left(A_b/A_g\right)\left(Ne^2/m\varepsilon_0\gamma\right) \tag{7}$$

N is the average electron density in the beam and A_b/A_g is a "filling factor" equal to the ratio of the beam cross-sectional area to the waveguide cross-sectional area and thus allows, in an approximate way, for the partial filling of the waveguide by the electrons. Equation 6 is exact for the case of a uniform beam completely filling the waveguide. Measurements of the beam current and beam profile yield ω_{pe}, and its values are given on line 8 of Table 1.

The growth rate of the cyclotron maser instability is <u>maximum</u>[8] when the group velocity $v_g=\partial\omega/\partial k_{\parallel}$ of each wave given by Eqs. 4 and 5 equals the electron beam velocity $\beta_{\parallel}c$. Solving Eqs. 4 and 5 simultaneously subject to the constraint that $v_g=\partial\omega/\partial k_{\parallel}=\beta_{\parallel}c$, leads to the following expression for the wave frequency at maximum growth rate:

$$\omega = (\gamma/s\Omega_0)\omega_c^2 \qquad (s = 1,2,3\ldots) \tag{8}$$

We see that the emission frequency is completely determined by the total beam energy γ, the critical axial magnetic field B_z and the cutoff frequency ω_c of Eq. 6, quantities that are known, or have been measured. Thus, we can compare the observed resonant frequencies, like those shown in Fig. 4 and 5, with those predicted by Eq. 8. Figure 6 illustrates this comparison. If the agreement had been perfect, all points would lie on the 45° dashed line. We see that the agreement is good. We note that at low frequencies, below 40GHz, the cyclotron maser interaction is

with the fundamental (s=1) gyrofrequency, whereas the 75GHz resonance corresponds to the second harmonic s=2, and the 113GHz resonance corresponds to the third harmonic s=3. The peak at 93GHz seen in Fig. 5 has not been identified.

The simultaneous solution of Eqs. 4 and 5 together with the constraint $\partial\omega/\partial k_{\parallel}=\beta_{\parallel}c$, yields yet another result of considerable interest, namely the ratio a of the perpendicular to parallel electron energies averaged over the beam cross-section:

$$a \equiv \gamma_{\perp}/\gamma_{\parallel} = \gamma^{1/2}\left[\frac{\omega}{s\Omega_0}(1+\gamma^2) - \gamma\right]^{-1/2} \qquad (9)$$

where $\gamma_{\perp}\equiv(1-\beta_{\perp}^2)^{-1/2}$ and $\gamma_{\parallel}\equiv(1-\beta_{\parallel}^2)^{-1/2}$. Since ω and s have been determined (see Fig. 6) and Ω_0 and γ are known, the ratio $a\equiv\gamma_{\perp}/\gamma_{\parallel}$ can be computed. The results are tabulated on line 10 of Table 1. We see that $\gamma_{\perp}/\gamma_{\parallel}$ falls within a small range between 0.5 and 0.7 for all our experiments. Observe the considerable perpendicular energy carried by the beam electrons. These values are not unreasonable for beams produced in foilless electron guns. By their very geometry the strong electric fields transverse to the axial magnetic field can cause significant cross-field motion which adds perpendicular energy to the beam electrons. A direct determination of $\gamma_{\perp}/\gamma_{\parallel}$ is difficult and has not been attempted by us. Nonetheless, estimates based on Eq. 9 provide one with a crude beam diagnostic.

So far we have concerned ourselves with the emission frequencies of the cyclotron maser instability, that is with the real part of the dispersion characteristics. The remainder of this section is devoted to a discussion of the emitted power, which is related to the imaginary part of the dispersion.

In the linear regime of the instability in which we operate (the theoretical saturated power level is ~70MW, approximately two orders in magnitude in excess of observed power levels), the power P grows exponentially with distance z along the drift tube and varies as

$$P = P_0 \exp[2\Gamma z]. \tag{10}$$

Here Γ is the maximum spatial growth rate, $\mathrm{Im}(\omega)/v_g$, and is given by the expression,[9]

$$\Gamma = \frac{3^{1/6}}{2v_g}\left[\frac{\omega_{p0}^2 Q^2 \omega_c}{\gamma}\,\frac{a}{(a^2+1)^{3/2}}\,\frac{(a^2\gamma^2-1)(\gamma^2+1)^{1/2}}{\gamma^3}\right]^{1/3} \tag{11}$$

where $a=\gamma_\perp/\gamma_\parallel$, $\omega_{p0}=(Ne^2/m\varepsilon_0)^{1/2}$ is the nonrelativistic plasma frequency, and Q^2 is a dimensionless coefficient dependent on the waveguide mode in question, and proportional to the beam cross-sectional area.

We have measured the radiated power P in the Ka-band range of frequencies (system 4 of Table 1) as a function of beam energy γ. The power is found to be a strong function of γ, and increases monotonically by two orders in magnitude, as γ is varied from ~2.2 to ~3.6. We now compare these observations with predictions based on Eqs. 10 and 11. To do so we assume that, as γ is varied, the cyclotron maser interaction frequency remains well within the spectrum of unstable wave numbers of the fastest growing mode. For γ=3.6 this mode was previously identified as the TE_{21} mode.

A measurement of beam current as a function of γ shows that the quantity I/γ is invariant. As a result, the effective plasma frequency of Eq. 7, and therefore ω_c of Eq. 6, are constant. In addition, the quantity $\omega_{p0}^2 Q^2/\gamma$ is constant since Q^2 is proportional to the beam area. In accordance with earlier discussions we may

assume that $a=\gamma_\perp/\gamma_\parallel$ is invariant and we set it equal to 0.5 (see Table 1). As a result, Γ of Eq. 11 can be written in the form

$$\Gamma = K\left[\left(a^2\gamma^2 - 1\right)\left(\gamma^2 + 1\right)^{1/2}\right]^{1/3}/\gamma \qquad (12)$$

which exhibits the complete dependence of the growth rate on beam energy γ, with K as a constant. A plot of this function is shown as the solid line of Fig. 7. The open circles are experimental points obtained from the measurements of power versus γ described above, and through the use of Eq. 10. The agreement is good. We point out that the experimental and theoretical data of Fig. 7 are normalized to each other at one point, which yields a value of P_0 equal to 7.1W (see Eq. 10). Since the emitted power P is 400kW (see Table 1), it follows from Eq. 10 that $2\Gamma z \simeq 11$, and the radiation has exponentiated through ~11 e-foldings. Suppose the radiated power were 4MW instead of 400kW, a ten-fold enhancement. This would require a value of $2\Gamma z$ of 13.2 instead of 11, and represents a 20% increase in the growth rate. Thus, a relatively modest increase in Γ can change the power level dramatically, a fact which has considerable bearing on our discussion in the next section. There we shall argue that the presence of a periodic transverse magnetic field superposed on the guiding field increases $\gamma_\perp$, and thus the intensity level of the cyclotron maser radiation.

IV. SPECTRAL STUDIES IN A COMBINED AXIAL MAGNETIC FIELD AND A PERIODIC TRANSVERSE FIELD (WIGGLER)

To generate a periodic transverse field,[10] the solenoid is loaded with a periodic assembly of copper rings, separated by Plexiglas rings as is illustrated in Fig. 8. The solenoid is powered by a capacitor bank which supplies a current pulse in the

shape of half a sine wave. Since the copper rings are good electrical conductors, the magnetic field diffuses gradually through them. On the other hand, the Plexiglas rings are insulators, and the magnetic field penetrates almost instantaneously. Thus the magnetic field is stronger in a Plexiglas ring and weaker in a copper ring. When the solenoid is empty, it produces a uniform, purely axial field B_z. Putting in the rings introduces a modulation in B_z, but in order to keep $\nabla.\vec{B}=0$, a radial magnetic field B_r is also generated. Note, however, that the field in the drift tube is primarily axial and therefore the same solenoid also provides the field which guides the electrons. We note that the fields change on a time scale of milliseconds. This means that during the short time (tens of nanoseconds) the pulsed, relativistic electron beam is on, the magnetic fields are essentially constant. Also, by varying the time during the magnet pulse at which the beam pulse is turned on, and by varying the charging voltage on the solenoid capacitor bank, the radial field B_r and the spatially averaged axial field B_z can be varied at will, independently of each other. The 70cm long wiggler section has been operated with periodicities ℓ of 4 and 6cm and amplitudes of B_r varying from zero to approximately 1kG.

Figure 9 shows the variation of microwave power as a function of the wiggler amplitude B_r measured in the 75-140GHz frequency range. The axial magnetic field B_z was held constant close to the critical value for peak power emission in the absence of the wiggler field (see section III). We see that the radiated power increases by a factor of 50 as the wiggler amplitude is increased from zero to 500G. The decrease in power at large wiggler amplitudes is believed to be due to the observed decrease in beam cur-

rent. Similar results to these were obtained also in the 26-40 GHz frequency range.

Figure 10 illustrates the radiation spectrum obtained with the grating spectrometer for fixed values of B_z and B_r. Comparing Fig. 10 with Fig. 5 (which was taken in the absence of the wiggler) one sees that the locations and relative magnitudes of the spectral features are the same even though the absolute power level has increased by about a factor of 20. The same behavior is also observed in the 26-40GHz frequency range.

We find throughout our measurements that the spectral characteristics of the radiation are preserved at all wiggler amplitudes we have used. Thus, we must attribute the increase in power to the enhanced growth rates of the cyclotron maser modes due to the transverse velocity induced by the wiggler field. This enhancement in the growth rate enters through the term $a=\gamma_\perp/\gamma_\parallel$ of Eq. 11. Although the precise details of the enhancement have not been worked out analytically, we know that an electron with initially zero perpendicular velocity entering a combined wiggler and guiding field acquires a transverse velocity given approximately by[11,12]

$$\frac{\beta_\perp}{\beta_\parallel} \approx \left(\frac{\Omega_r}{\Omega_0}\right)\left[\frac{k_0 c\gamma\beta_\parallel}{\Omega_0} - 1\right]^{-1} \qquad (13)$$

where $\Omega_0=eB_z/m_0$, $\Omega_r=eB_r/m_0$ and $k_0=2\pi/\ell$, with ℓ as the wiggler period. Since steady magnetic fields do no work, the values of $\beta_\perp$ and $\beta_\parallel$ given by the above equation are subject to the energy conservation equation $\beta_\perp^2+\beta_\parallel^2=(1-\gamma^{-2})$ = constant. We note that a resonant enhancement of $\beta_\perp$ occurs when $k_0 c\gamma\beta_\parallel/\Omega_0=1$ in which situation the electron-cyclotron and wiggler frequencies are equal

when observed in the rest frame of the drifting electrons. We have looked for a corresponding enhancement in the microwave emission, but to no avail. Indeed, at the resonance which occurs at $B_z \simeq 6.5$kG for the conditions of our experiment, a pronounced minimum in power is measured, both with and without the wiggler field. A similar minimum in the emitted power has been reported recently by other workers.[13] It may well be that at and near resonance, the particle orbits become unstable[14,15] causing a disruption of the coherent emission processes. However, if this is so, the particle orbits have not become sufficiently violent as to cause macroscopic changes in the beam dynamics, since a pronounced change in beam current has not been observed.

V. CONCLUSIONS

In conclusion, then, millimeter wave radiation at power levels as high as 2MW, generated by the electron-cyclotron maser instability has been observed from electron beams propagating in uniform, guiding magnetic fields. The rotational free energy necessary for the instability is supplied by the foilless, magnetron injection type of gun used. We infer from the experiments that the ratio $\gamma_\perp/\gamma_\parallel$ averaged over the beam cross section is typically 0.5.

We have identified several modes of the maser instability whose frequencies agree well with those predicted from theory, under maximum growth rate conditions. The functional dependence of the intensity on beam energy agrees well with that inferred from the linear growth rate of the cyclotron maser instability.

In the presence of a periodic wiggler field, the radiation intensity is increased by one to two orders in magnitude. Since the spectra remain otherwise unchanged, we conclude that the role

of the wiggler is to enhance the cyclotron maser instability by virtue of adding more perpendicular momentum to the electrons. However, an analysis of this problem has not been made because the theory of the cyclotron maser instability in a combined guiding and wiggler field is not presently available.

Because of the dominant role played by the cyclotron maser instability, we have not been able to identify spectral features attributable to the free electron laser mechanism. We feel that our observations are relevant to those of other experimenters[16] who used foilless guns similar to ours, but who, not having studied the low-level spectral characteristics of the emission at zero wiggler fields, interpret their results in terms of three-wave, Raman, free electron laser phenomena.

REFERENCES

1. M. Friedman and M. Herndon, Phys. Fluids 16, 1982 (1973); V.L. Granatstein, M. Herndon, R.K. Parker, and S.P. Schlesinger, IEEE Trans. Microwave Theory Tech. MTT-2, 1000 (1974); V.L. Granatstein, P. Sprangle, R.K. Parker, and M. Herndon, J. Appl. Phys. 46, 2021 (1975); V.L. Granatstein, P. Sprangle, M. Herndon, R.K. Parker, and S.P. Schlesinger, J. Appl. Phys. 46, 3800 (1975); V.L. Granatstein, M. Herndon, P. Sprangle, Y. Carmel, and J.A. Nation, Plasma Physics 17, 23 (1975); P.C. Efthimion and S.P. Schlesinger, Phys. Rev. A 16, 633 (1977); G. Providakes and J.A. Nation, J. Appl. Phys. 50, 3026 (1979); T.C. Marshall, S. Talmadge, and P. Efthimion, Appl. Phys. Lett. 31, 320 (1977); R.M. Gilgenbach, T.C. Marshall, and S.P. Schlesinger, Phys. Fluids 22, 971 (1979); D.B. McDermott, T.C. Marshall, and S.P. Schlesinger, Phys. Rev. Lett. 41, 1368 (1978).

2. K.R. Chu and J.L. Hirshfield, Phys. Fluids 21, 461 (1978); J.L. Hirshfield, K.R. Chu, and S. Kainer, Appl. Phys. Lett. 33, 847 (1978); E. Ott and W.M. Manheimer, IEEE Trans. Plasma Sc. PS-3, 1 (1975); P. Sprangle and W.M. Manheimer, Phys. Fluids 18, 224 (1975); V.L. Bratman and A.E. Tokarev, Radiophysics and Quantum Electronics 17, 932 (1974); H.S. Uhm, R.C. Davidson, and K.R. Chu, Phys. Fluids 21, 1866 (1978); H.S. Uhm, R.C. Davidson, and K.R. Chu, Phys. Fluids 21, 1877 (1978); K.R. Chu, Phys. Fluids 21, 2354 (1978); H.S. Uhm and R.C. Davidson, J. Appl. Phys. 50, 696 (1979); P. Sprangle and A.T. Drobot, IEEE Trans. Microwave Theory Tech. MTT-25, 528 (1977).

3. P. Sprangle, R.A. Smith, and V.L. Granatstein, NRL Memorandum Report 3911, Dec. 8, 1978 and Infrared and Millimeter Waves -

Vol. 1, p. 279, ed. K.J. Button, Academic Press (1979) and references therein.

4. M. Friedman and M. Ury, Rev. Sci. Instrum. 41, 1334 (1970); M.E. Read and J.A. Nation, J. Plasma Phys 13, 127 (1975).

5. T.J. Orzechowski and G. Bekefi, Phys. Fluids 22, 978 (1979).

6. J.A. Pasour and S.P. Schlesinger, Rev. Sci. Intrum. 48,1355 (1977).

7. J.M. Buzzi, K. Felch, and L. Vallier, Bull. Am. Phys. Soc. 25, 887 (1980).

8. P. Sprangle and A.T. Drobot, IEEE Trans. Microwave Theory and Techniques, MTT-25, 528 (1977).

9. H.S. Uhm, R.C. Davidson, and K.R. Chu, Phys. Fluids 21, 1877 (1978).

10. K.D. Jacobs, R.E. Shefer, and G. Bekefi, Appl. Phys. Lett. 37, 583 (1980); also K.D. Jacobs, G. Bekefi, and J.R. Freeman, M.I.T. Plasma Fusion Center Report No. PFC/JA-81-2 January 1981.

11. L. Friedland, Phys. Fluids 23, 2376 (1980).

12. K.D. Jacobs and G. Bekefi, Proc. IEEE International Conference on Plasma Science, Santa Fe, NM 1981, page 47.

13. S.H. Gold, R.H. Jackson, R.K. Parker, V.L. Granatstein, M. Herndon, and A.K. Kinkead, Proc. IEEE International Conference on Plasma Science, Santa FE, NM 1981, page 46.

14. P. Diament, Phys. Rev. A23, 2537 (1981).

15. H.P. Freund and A.T. Drobot "Relativistic Electron Trajectories in Free Electron Lasers with an Axial Guide Field" (to be published).

16. P.C. Efthimion and S.P. Schlesinger, Phys. Rev. A16, 633 (1977); R.M. Gilgenbach, T.C. Marshall, and S.P. Schlesinger, Phys. Fluids 22, 971 (1979); R.M. Gilgenbach, T.C. Marshall, and S.P. Schlesinger, Phys. Fluids 22, 1219 (1979); D.B. McDermott, T.C. Marshall, S.P. Schlesinger, R.K. Parker, and V.L. Granatstein, Phys. Rev. Lett. 41, 1368 (1978); G. Providakes, and J.A. Nation, J. Appl. Phys. 50, 3026 (1979); A.N. Didenko, A.R. Borisov, G.R. Fomenko, A.V. Kozevnikov, G.V. Melnikov, Yu. G. Stein, and A.G. Zerlitsin, IEEE Trans. Nuclear Science, NS-28, 3169 (1981).

TABLE 1. SUMMARY OF SYSTEM PARAMETERS

(Items marked with an asterisk refer to values measured at maximum microwave power emission and zero wiggler amplitude).

PARAMETER	System 1	System 2	System 3	System 4	System 5
Frequency Range	8-12 GHz	8-12 GHz	26-40 GHz	26-40 GHz	75-140 GHz
Waveguide	cylindrical	coaxial	cylindrical	coaxial	cylindrical
Spectrum Analysis	dispersive line	dispersive line	dispersive line	dispersive line	grating spectrometer
Crystal Detectors	H.P. 423A	H.P. 423A	H.P. R422A	H.P. R422A	H.P. R422A
Axial B Field* (kG)	5.5	~4.7	7.5	8.9	9.4
$\gamma^* = 1 + (eV/m_0c^2)$	2.84	2.80	3.53	3.54	3.18
Effective $\omega^*_{pe}/2\pi$ (GHz)	—	1.61	4.11	2.47	3.97
Microwave Power* (kW)	—	20	1500	400	60
$\gamma_\perp/\gamma^*_\parallel$	0.67	0.72	0.50	0.54	0.50
Wiggler Field Amplitude (kG)	0	0	0	0 to 1.3	0 to 0.7
Wiggler Periodicity (cm)	—	—	—	6	4

CAPTIONS TO FIGURES

Fig. 1. (a) The experimental arrangement; (b) scale drawing of electron guns.

Fig. 2. Oscilloscope traces of the beam voltage, current and microwave signal.

Fig. 3. Microwave power emitted in the 75-140GHz frequency range as a function of the axial, guiding magnetic field B_z.

Fig. 4. Oscilloscope traces of signals received on dispersive lines operating in the 8-12GHz and 26-40GHz frequency regimes. a is the reference signal; b the dispersed signal.

Fig. 5. Spectrum in the 75-140GHz frequency regime measured with a millimeter-wave grating spectrometer.

Fig. 6. Observed resonant frequencies plotted against the calculated frequencies for the unstable cyclotron maser modes identified in the experiments.

Fig. 7. The growth rate Γ as a function of beam energy γ for an unstable TE waveguide mode.

Fig. 8. Cutaway view of the diffusive wiggler[10] which generates a periodic magnetic "mirror" field of the form $\vec{B}(r,z) \approx \hat{z}[B_z + b(r)\cos(k_0 z)] + \hat{r}\, B_r(r)\sin(k_0 z)$. $k_0 = 2\pi/\ell$ and ℓ is the period. $B_r = 0$ when $r=0$, and the axial magnetic field is modulated with amplitude $b(r)$. The wall thickness W of the first ring is reduced, which allows adiabatic injection of the electron beam.[3,10]

Fig. 9. Radiated power in the 75-140GHz frequency regime as a function of the radial magnetic amplitude B_r generated by the wiggler of Fig. 8. The period ℓ=4cm. The axial magnetic field B_z is held fixed at a value of 10kG.

Fig. 10. Measured spectrum in the 75-140GHz frequency regime at fixed values of the radial wiggler field B_r and axial guiding field B_z.

(a)

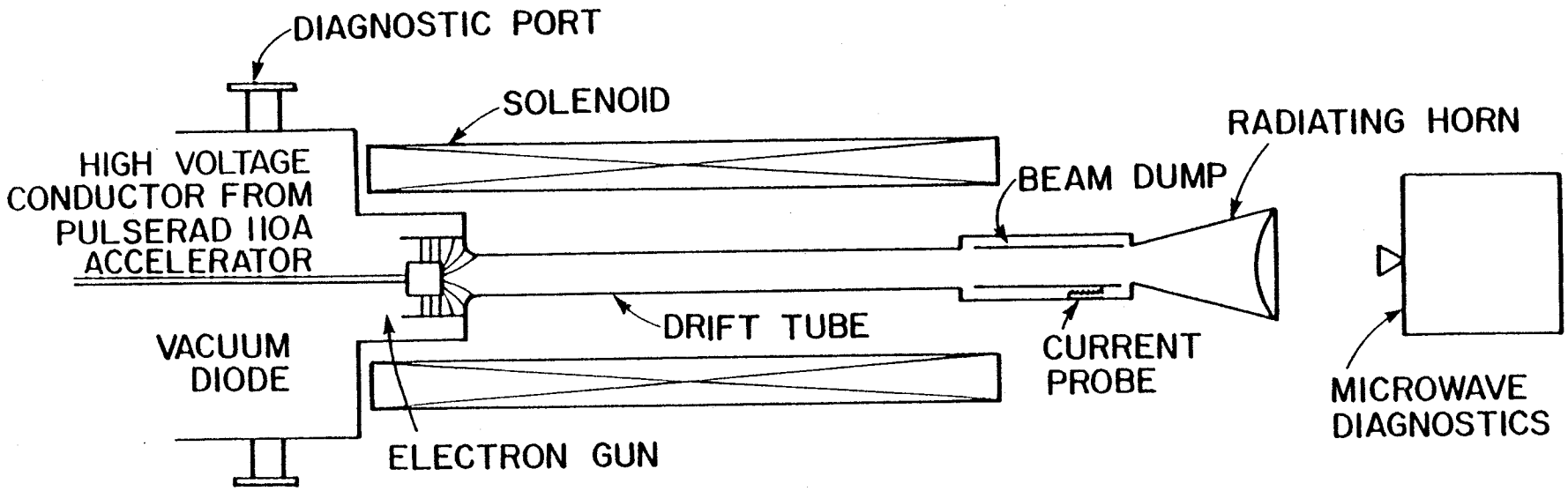

(b)

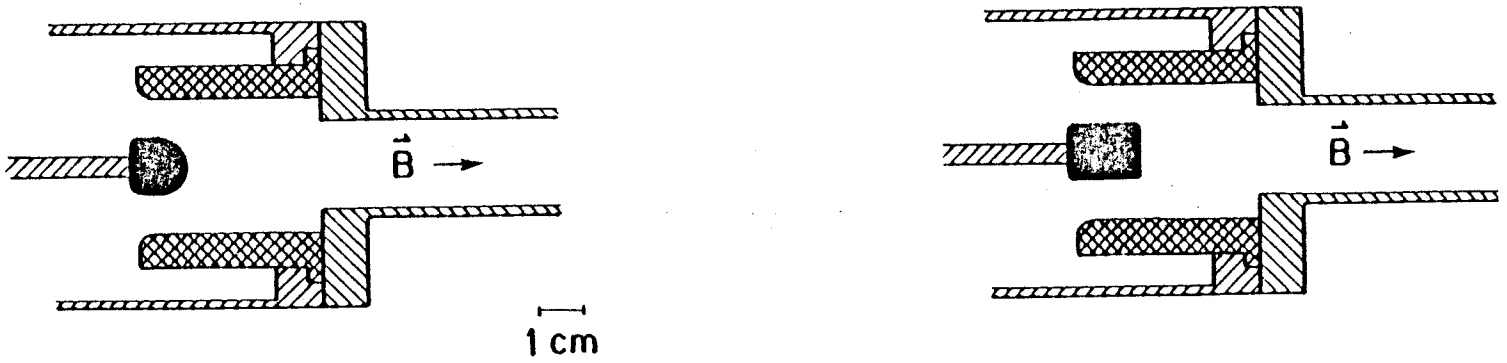

Fig.1 Shefer and Bekefi

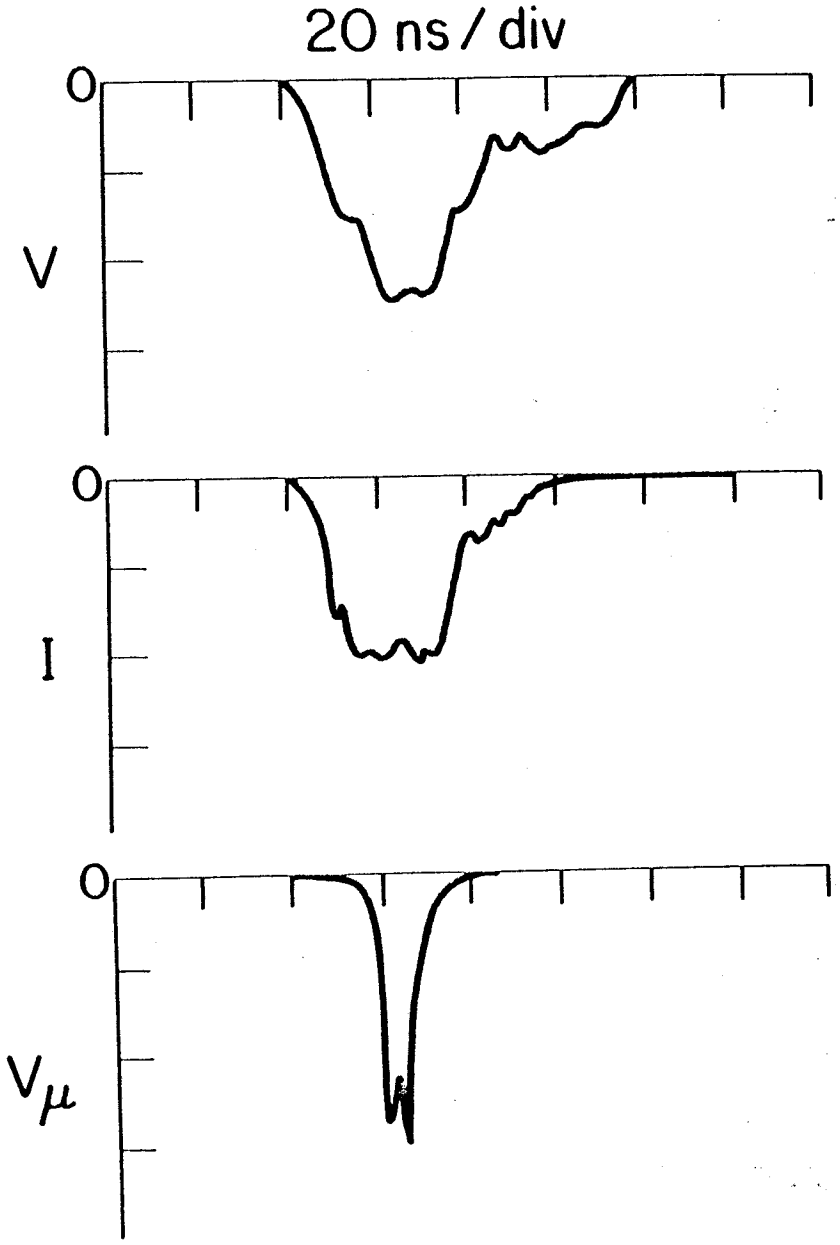

VOLTAGE
433 kV / div

BEAM CURRENT
4 kA / div

MICROWAVE
DETECTOR
5 mV / div

Fig.2 Shefer and Bekefi

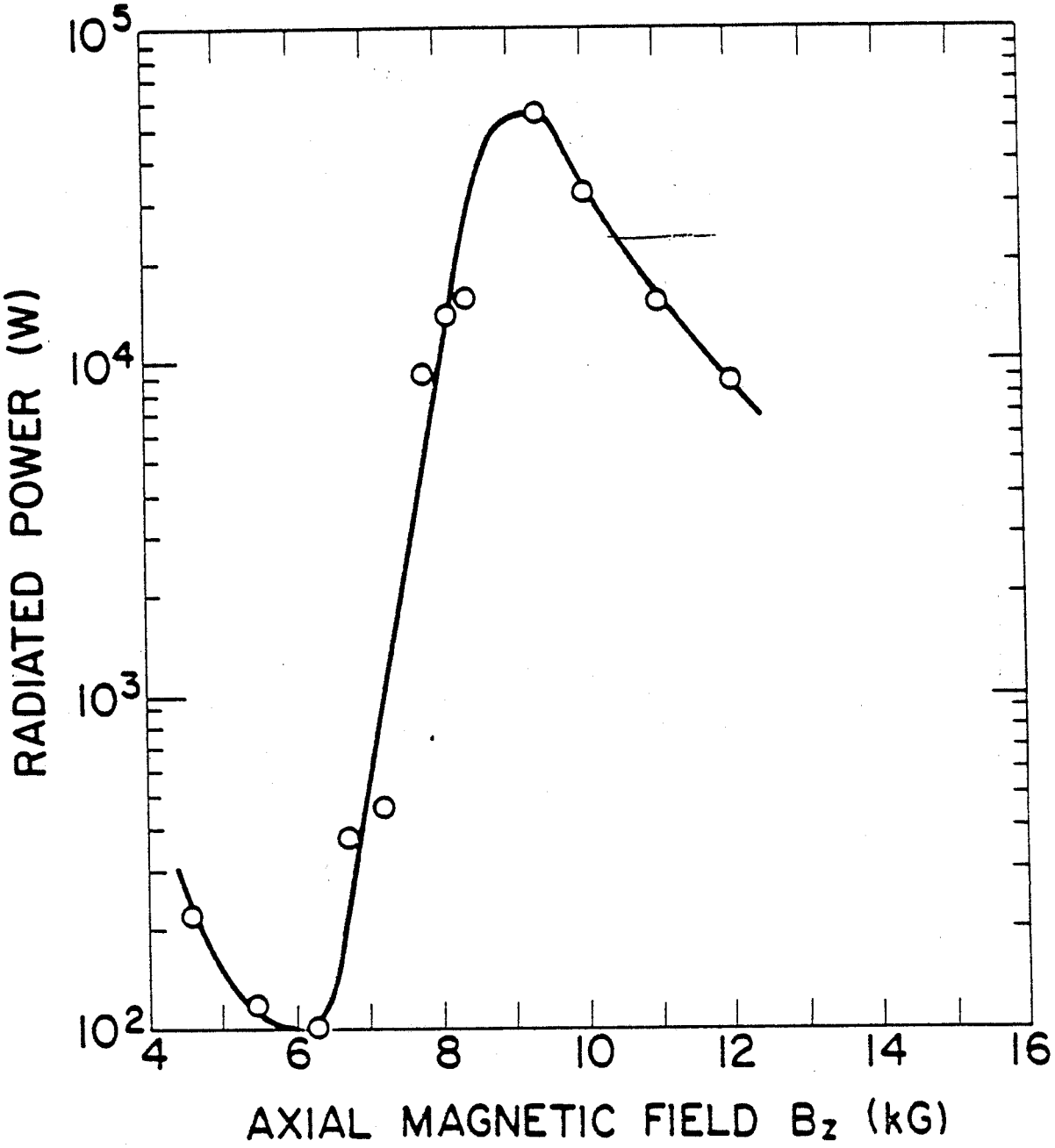
RADIATED POWER (W)
10^5
10^4
10^3
10^2
4
6
8
10
12
14
16
AXIAL MAGNETIC FIELD B_z (kG)

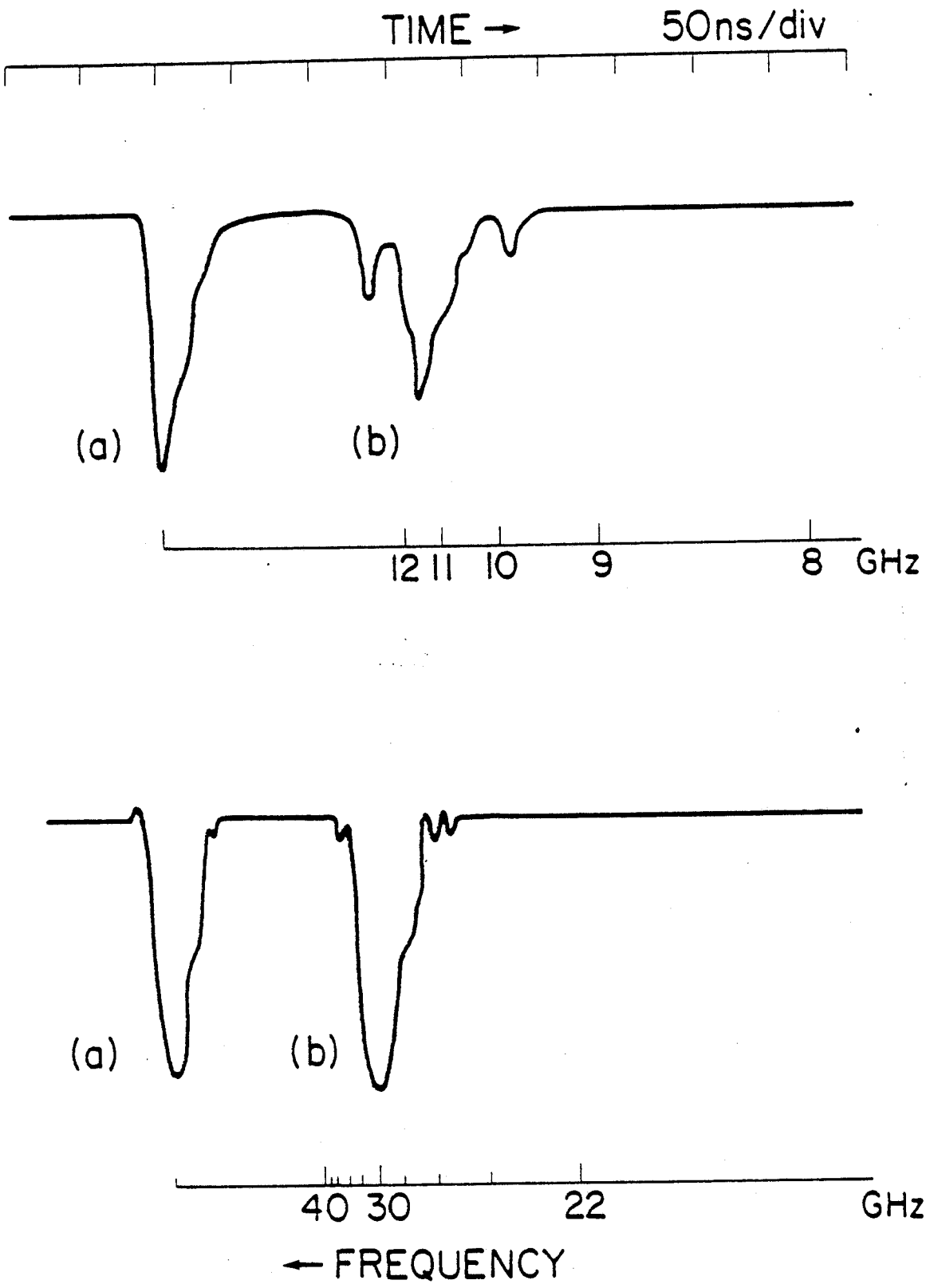

Fig,4 Shefer and Bekefi

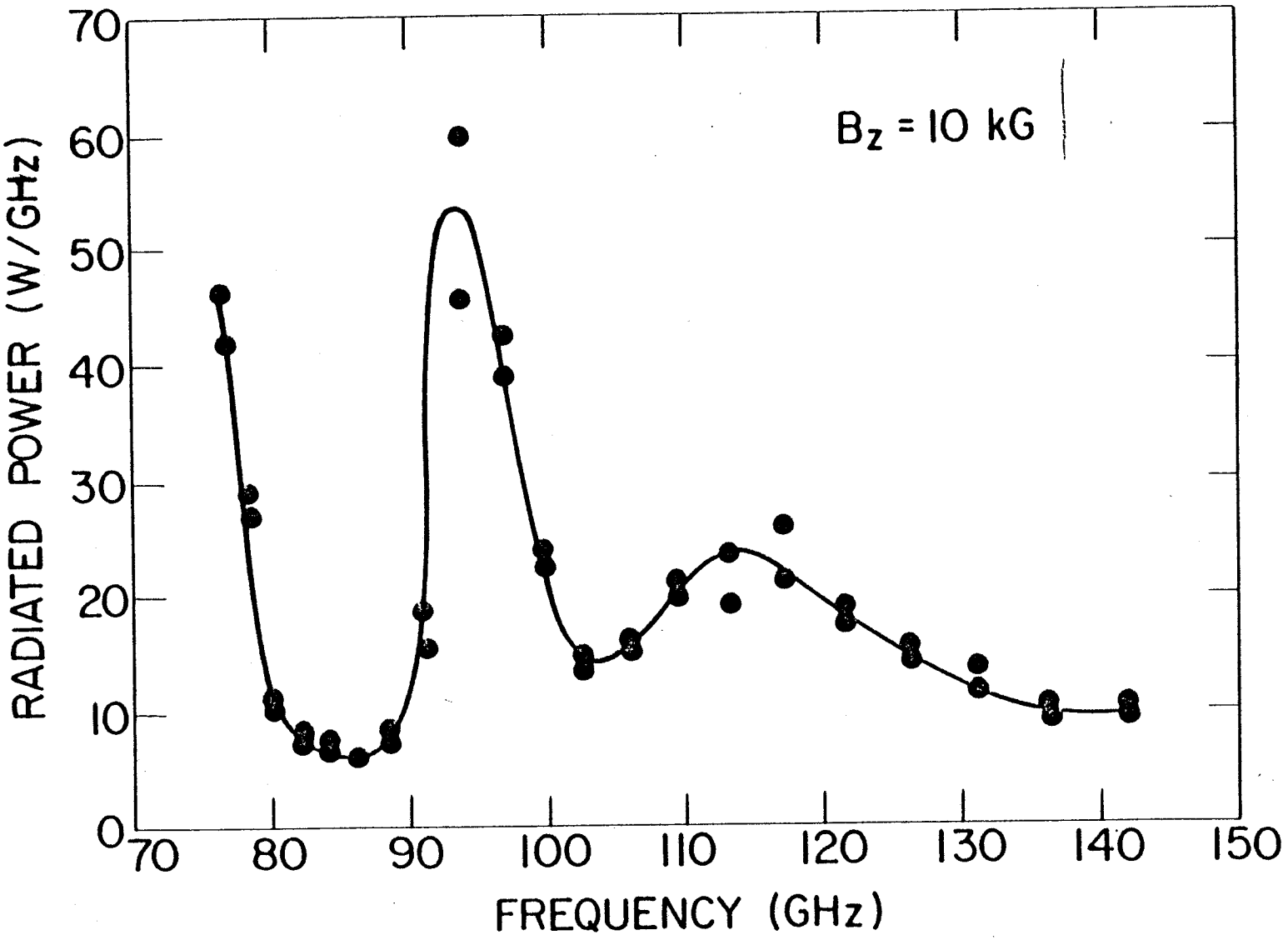

Fig.5 Shefer and Bekefi

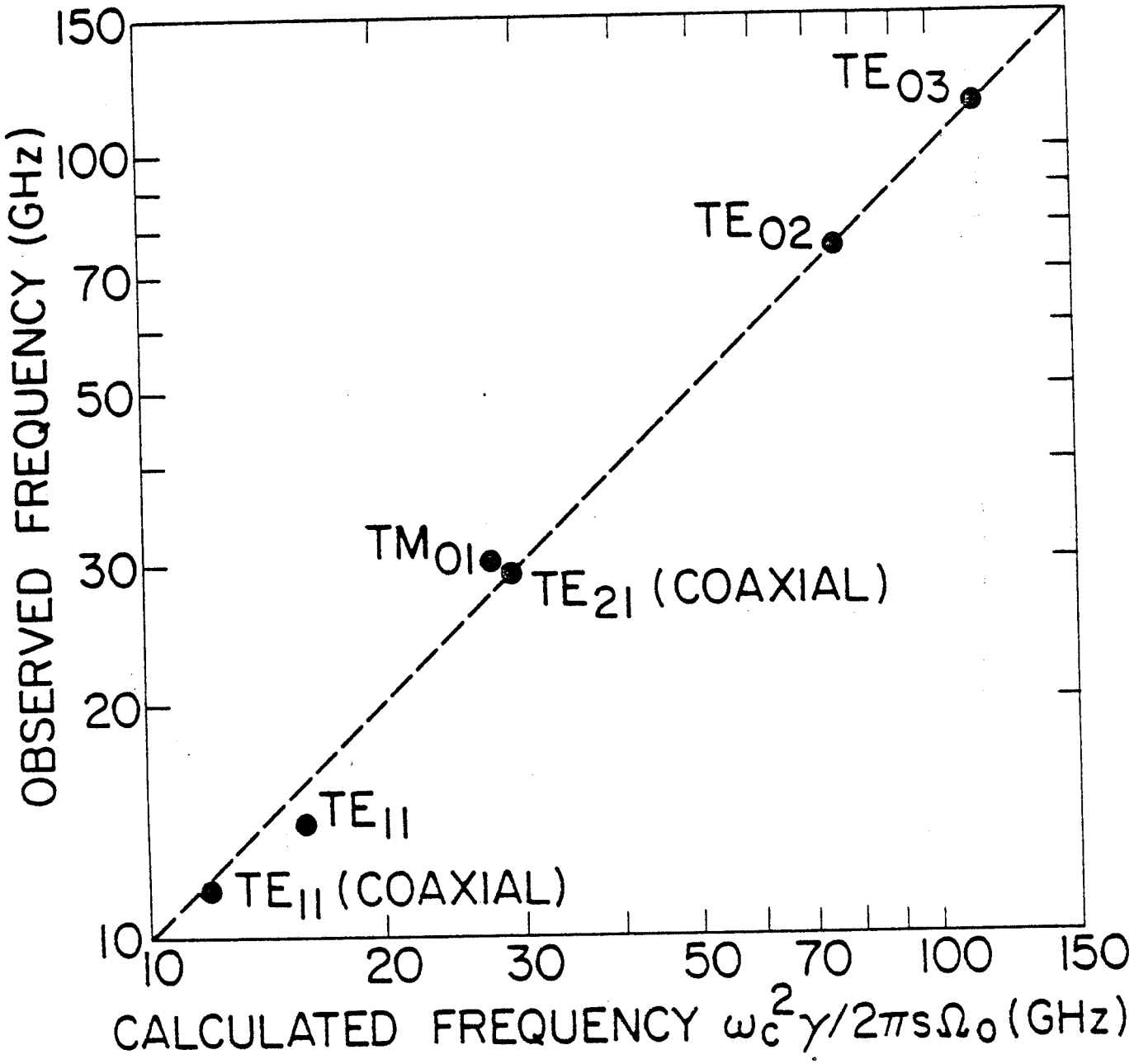

Fig.6 Shefer and Bekefi

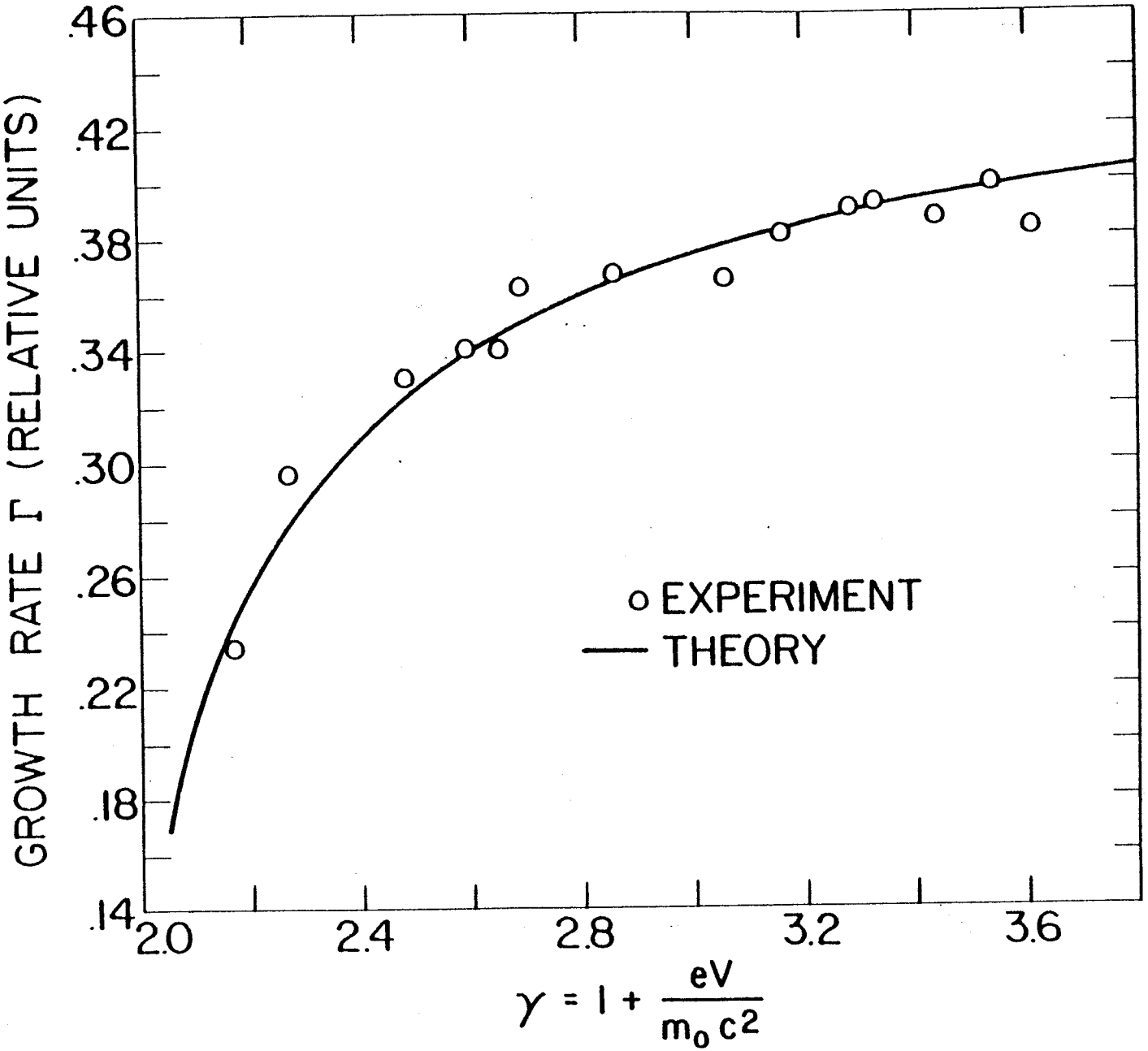

Fig.7 Shefer and Bekefi

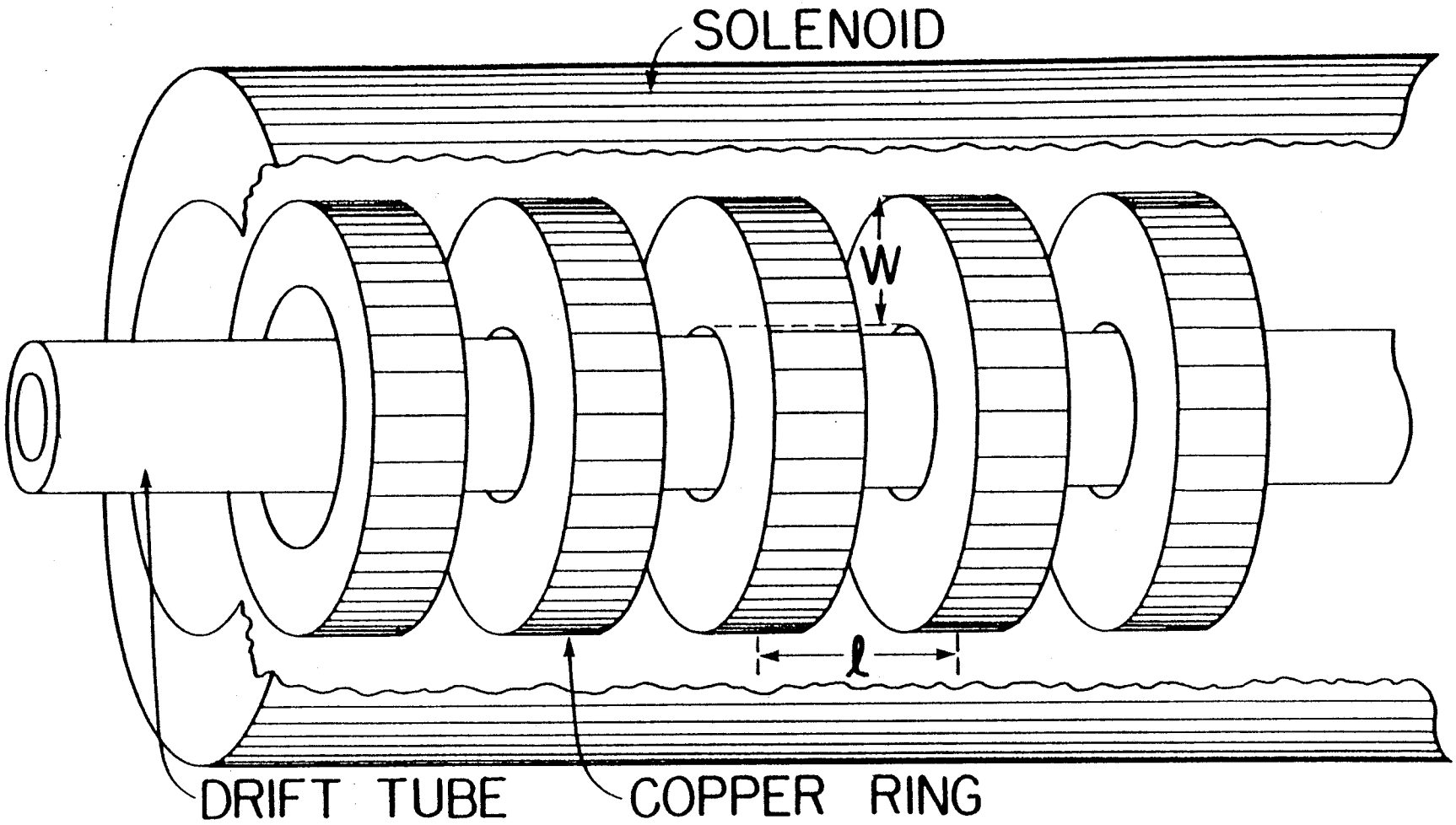

Fig.8 Shefer and Bekefi

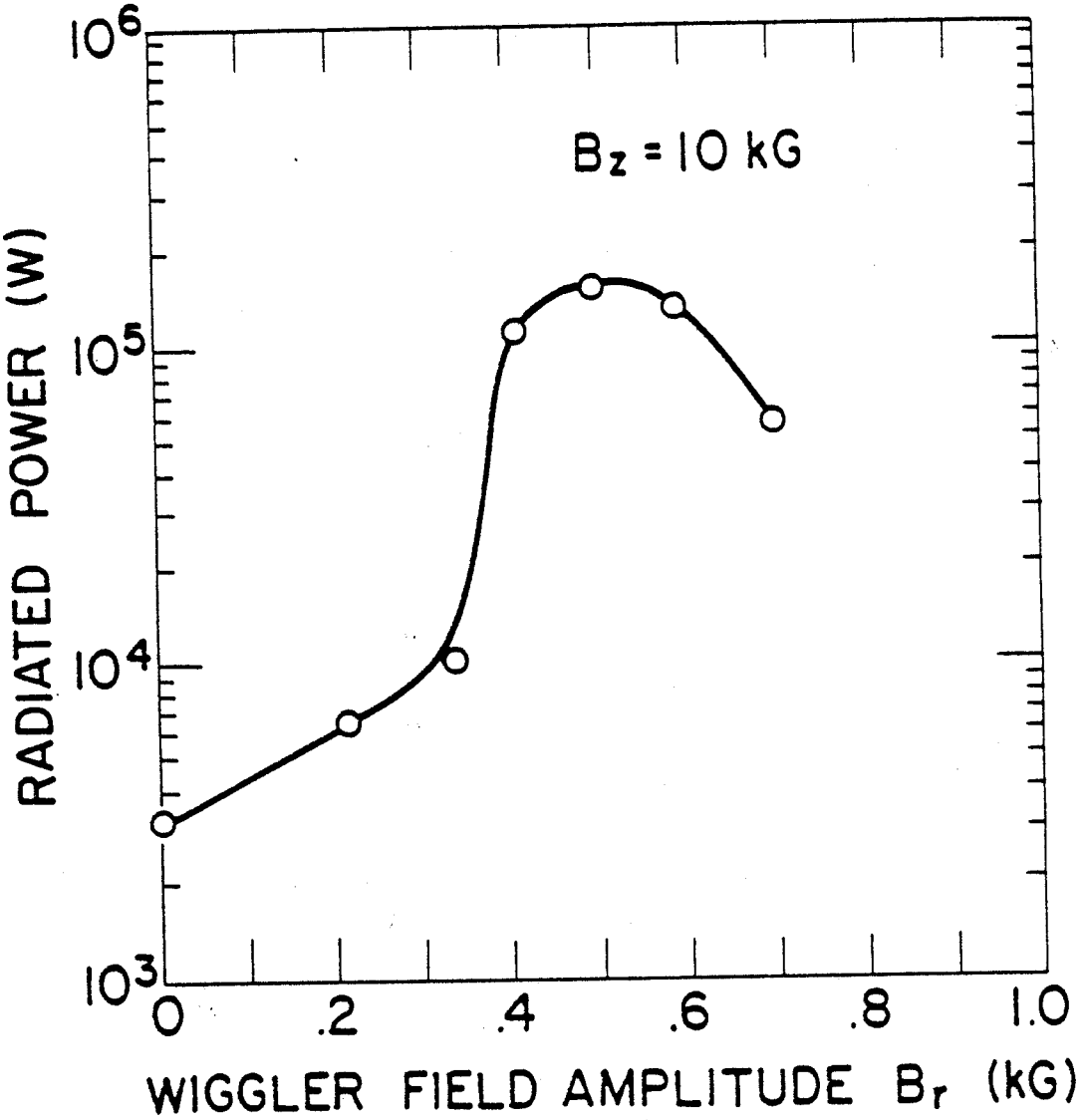

Fig,9 Shefer and Bekefi

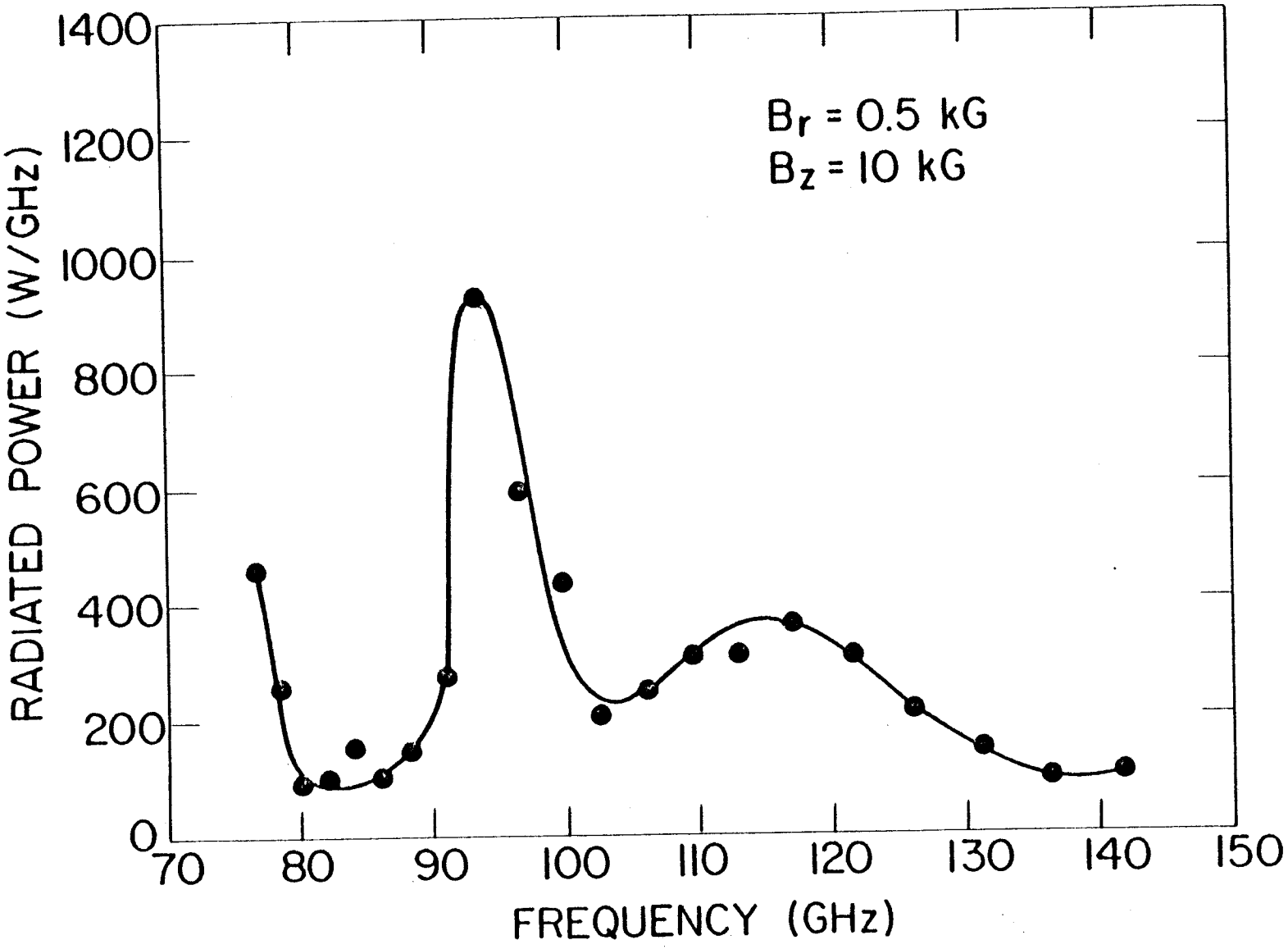

Fig.10 Shefer and Bekefi

ation in a conventional higher density ($\bar{n} > 10^{13}\,\mathrm{cm}^{-3}$) Maxwellian plasma. In view of these results, to achieve steady state RF driven operation at high density, it may be necessary to start up at low density, build up the RF current, and then raise the density by gas puffing or pellet injection. Additional RF power may also be necessary.

Acknowledgements

We thank PPPL for the loan of the klystron RF power source. Discussions with Drs. P. Bonoli and R. Englade regarding their unpublished theoretical works related to this subject are gratefully acknowledged.

REFERENCES

1. Furth, H.P., Nuclear Fusion 15, 487 (1975).
2. Clark, W.H.M., J.G. Cordey, M. Cox, R.D. Gill, J. Hugill, J.W.M. Paul and D.F.H. Start, Phys. Rev. Lett., 45, 1101 (1980).
3. Wort, D.J.H., Plasma Physics, 73, 258 (1971).
4. Fisch, N.J., Phys. Rev. Lett., 41, 873 (1978).
5. Fisch, N.J. and A. Bers, Proceedings of the 3rd Topical Conference on RF Plasma Heating, Pasadena, Calif. (1978).
6. Wong, K.L., Phys. Rev. Lett.,43, 438 (1979).
7. Wong, K.L, R. Horton and M. Ono, Phys. Rev. Lett., 45, 117 (1980).
8. Luxon, J.L. R.L. Freeman, V.S. Chan, S.I. Chiu, J.C. DeBoo, R.W. Harvey, T.H. Jensen, R.J. LaHay, J.M. Lohr, C.P. Moeller, T. Ohkawa, J.C. Riordan, J.F. Tooker, and D.F. Vaslow, GA-A15820.
9. Yamamoto, T, T. Imai, M. Shimada, N. Suzuki, M. Maeno, S. Konoshima, T. Fujii, K. Vehara, T. Nagashima, A. Funahashi, and N. Fujisawa, Phys. Rev. Lett., 45, 716 (1980).
10. Terumichi, Y., T. Maekawa, T. Shomozuma, T. Saito, M. Nakamura, T. Cho, S. Kubo, Y. Hamada, S. Tanaka, 4th Topical Conference on RF Plasma Heating, p. B11-1, Austin, Texas (1981).
11. Ohkubo, K., S. Takamura, K. Kawahata, T. Tetsuka, K. Matsuura, N. Noda, K. Sakuri, S. Tanahashi, J. Fujita, 4th Topical Conference of RF Plasma Heating, p. B4-1, Austin, Texas (1980).
12. Luckhardt, S.C., M. Porkolab, K.I. Chen, and S.F. Knowlton, 4th Topical Conference on RF Plasma Heating, p. B6-1 Austin, Texas (1980).
13. Oren, L., and R.J. Taylor, Nuclear Fusion, 17, 1143 (1977).
14. Coppi, B., F. Pegoraro, R. Pozzoli, G. Rewoldt, Nuclear Fusion, 16, 309 (1976).
15. Englade, R., T. Antonsen, M. Porkolab, P. Bonoli, and E. Ott, 2nd Joint Varenna-Grenoble International Symposium on RF Heating of Toroidal Plasmas, Como, Italy (1980).
16. Private communication P. Bonoli.

FIGURE CAPTIONS

Fig. 1 a. Superimposed signals with and without RF power: One turn loop voltage (V_L)0.8 volts/div., total current (I_t)$8kA$/div., RF power $30kW$/div.

b. Loop voltage with $dI/dt = 0$ at high RF power: loop voltage 0.4 volts/div., total current $4kA$/div. (baseline suppressed), RF power $30kW$/div.

c. Current increment ΔI_t normalized to RF power transmission coefficient T as a function of array phase $\Delta\phi$ with a 4 msec RF pulse. Plasma parameters, $I_t = 30kA$, $\overline{n} = 2 \times 10^{12}\text{cm}^{-3}$, $B_\phi = 8k\text{Gauss}$.

Fig. 2 Array phase dependence of (a) central electron temperature during RF pulse. The dashed line indicates temperature with no RF; (b) current increment ΔI_t normalized to RF power transmission coefficient, with 4 msec RF pulse length, $\overline{n}_e = 5 \times 10^{12}\text{cm}^{-3}$; (c) dependence of ΔI_t on line average density at beginning of RF pulse in units of 10^{12}cm^{-3} in type I discharges with deuterium plasma, $\Delta\phi = -90°$, $P_{RF} = 15kW$ (closed circles). Current increment in type II discharge (closed triangle).

Fig. 3 Signals with (solid) and without (dashed) applied RF power, $\Delta\phi = -90°$. (a) Total current (I_t) in kiloamps and loop voltage (V_{loop}) in volts; (b) ohmic heating power from inductively corrected loop voltage (P_{OH}) in kilowatts and RF power (P_{RF}); (c) central electron temperature in eV from two different runs. Open circles and triangles: no RF. Closed circles and triangles: RF applied. The triangular data points were taken with a 3 msec duration RF pulse. (d) Line average density $\overline{n}_e$ in units 10^{12}cm^{-3} and hard X-ray signal U_x in relative units.

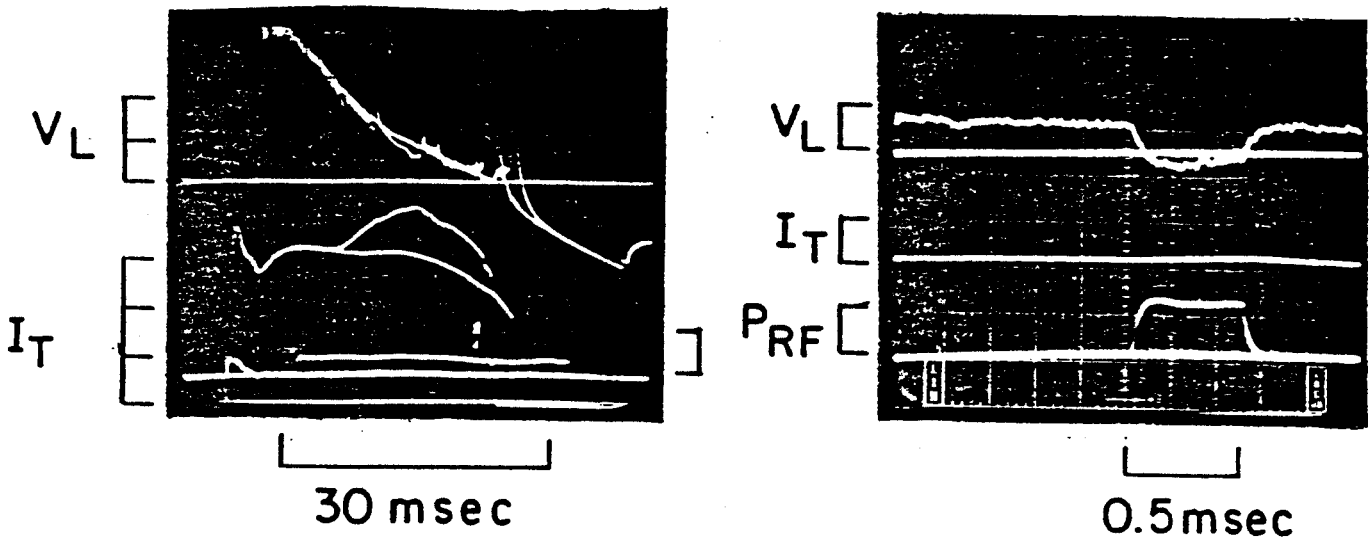
V_L
I_T
30 msec
V_L
I_T
P_{RF}
0.5msec

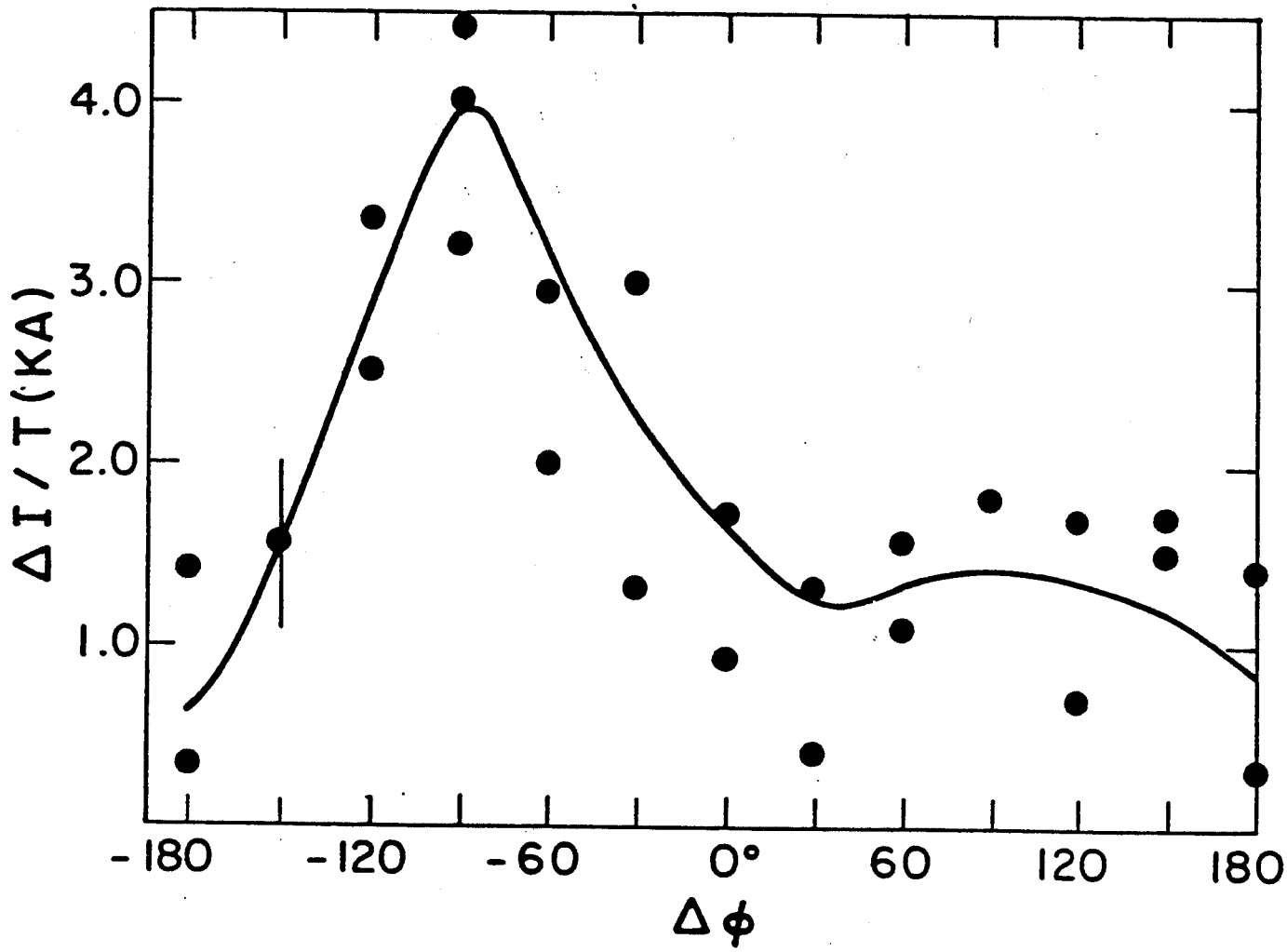
4.0
3.0
2.0
1.0
ΔI/T(KA)
-180
-120
-60
0°
60
120
180
Δφ

Fig. 1

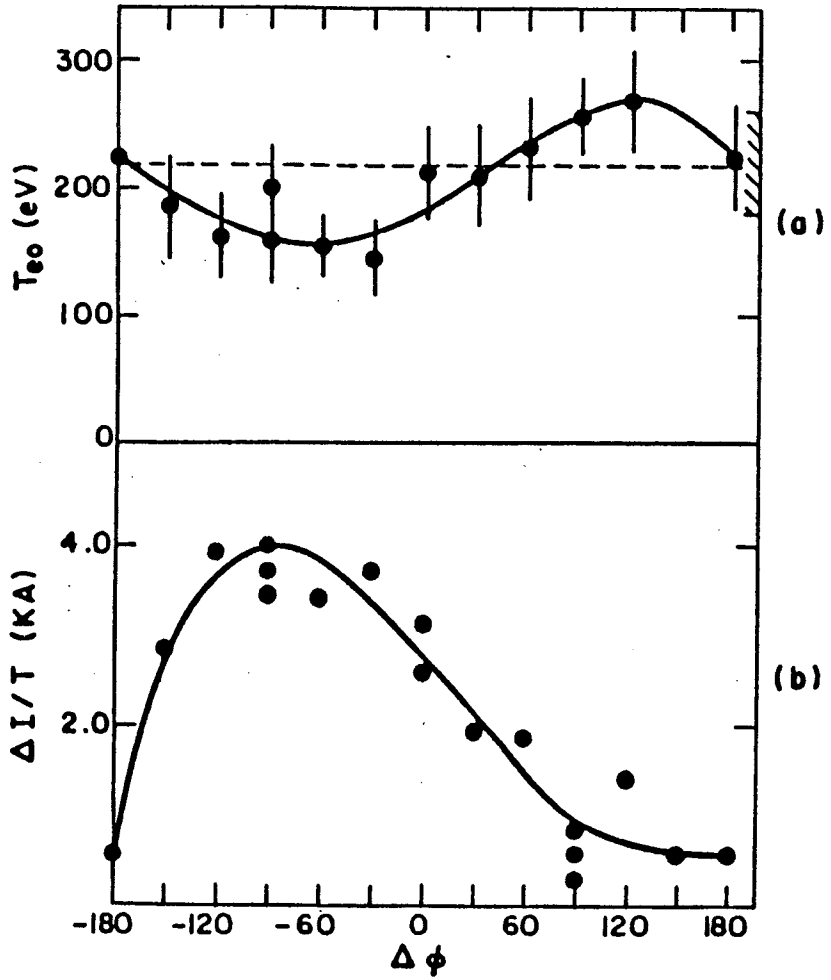
300
200
100
0
T_{eo} (eV)
(a)
4.0
2.0
$\Delta I/T$ (KA)
(b)
-180
-120
-60
0
60
120
180
$\Delta\phi$

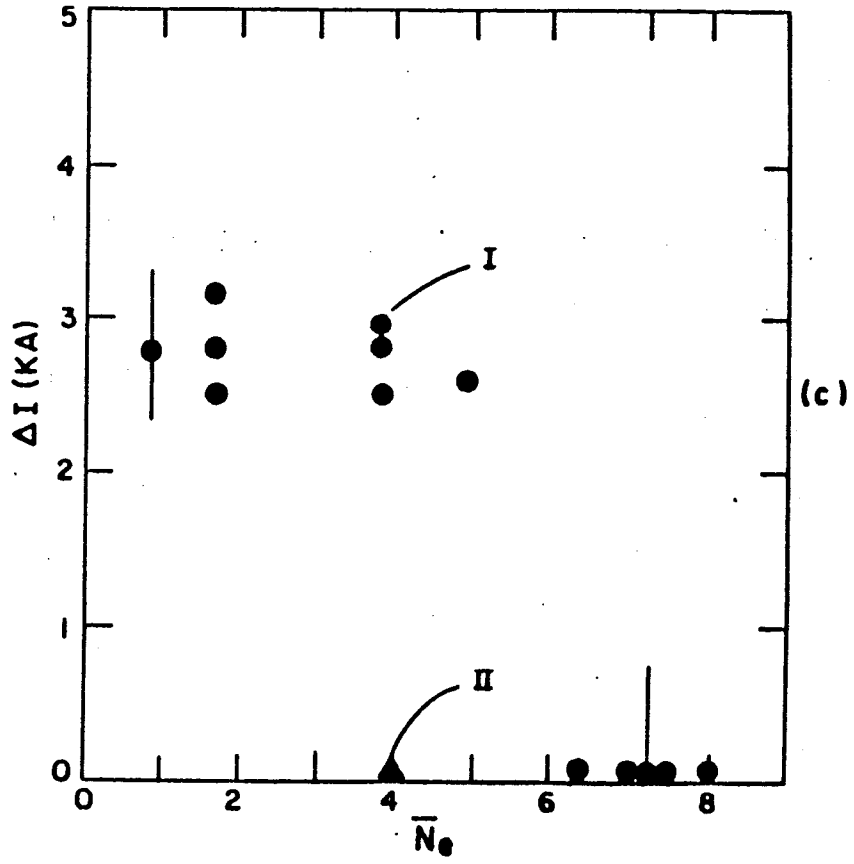
5
4
3
2
1
0
ΔI (KA)
I
II
(c)
0
2
4
6
8
$\bar{N}_e$

Fig. 2

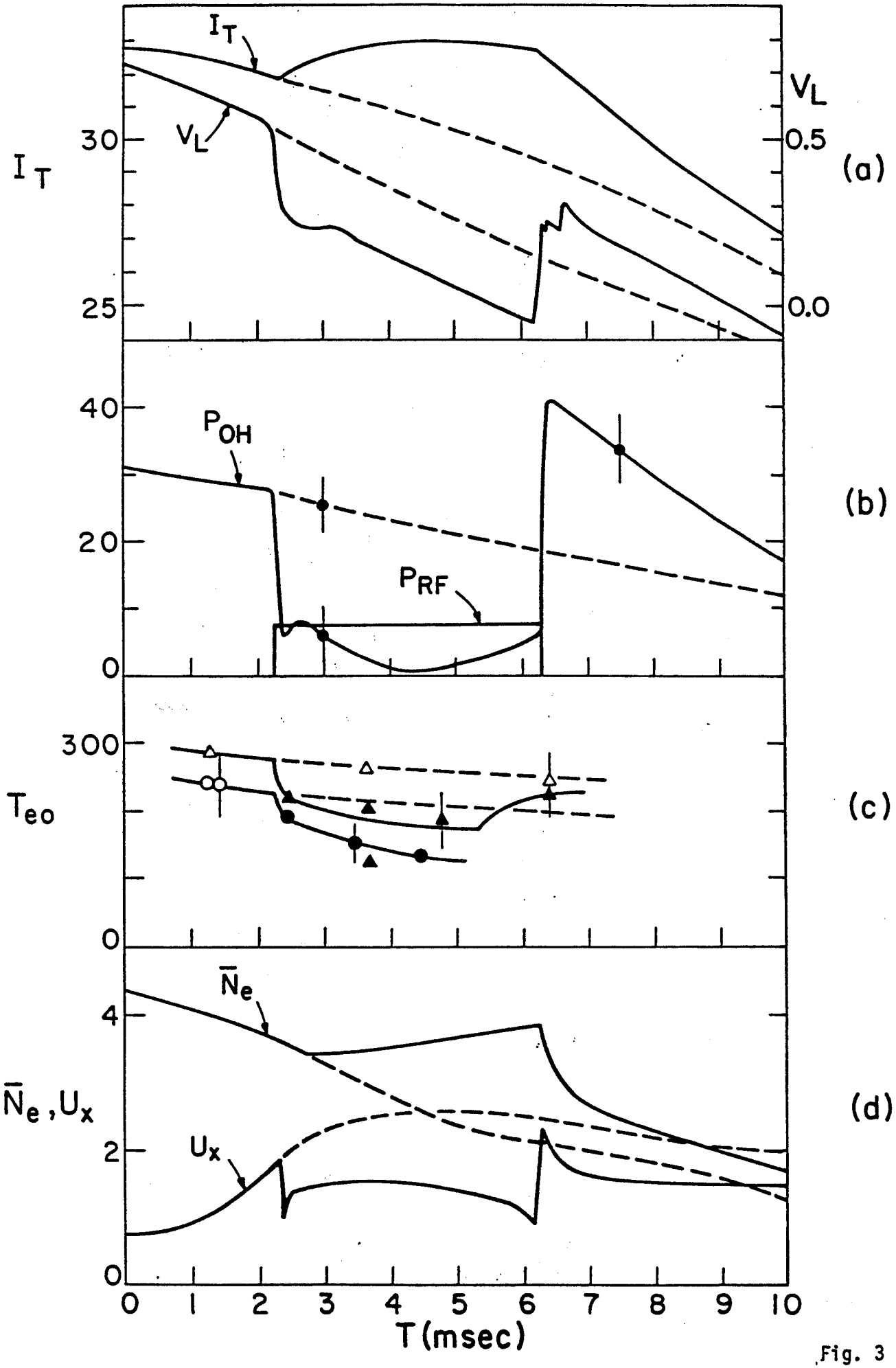
I_T
V_L
30
25
I_T
V_L
0.5
0.0
(a)
40
20
0
P_{OH}
P_{RF}
(b)
300
0
T_{eo}
(c)
$\bar{N}_e$
4
2
0
$\bar{N}_e, U_x$
U_x
(d)
0 1 2 3 4 5 6 7 8 9 10
T (msec)

Fig. 3